Adaptive Local Thresholding by Verification-Based Multithreshold Probing with Application to Vessel Detection in Retinal Images

Xiaoyi Jiang, *Member*, *IEEE Computer Society*, and Daniel Mojon

Abstract—In this paper, we propose a general framework of adaptive local thresholding based on a verification-based multithreshold probing scheme. Object hypotheses are generated by binarization using hypothetic thresholds and accepted/rejected by a verification procedure. The application-dependent verification procedure can be designed to fully utilize all relevant informations about the objects of interest. In this sense, our approach is regarded as knowledge-guided adaptive thresholding, in contrast to most algorithms known from the literature. We apply our general framework to detect vessels in retinal images. An experimental evaluation demonstrates superior performance over global thresholding and a vessel detection method recently reported in the literature. Due to its simplicity and general nature, our novel approach is expected to be applicable to a variety of other applications.

Index Terms—Adaptive local thresholding, threshold probing, hypotheses generation and verification, vessel segmentation, retinal imaging, medical imaging.

1 Introduction

Situations in which global thresholds do not work well are typically caused by poor quality of the source material, existence of multiple object classes of varying color/reflectance, nonuniform illumination, and camera distortions. Vessel detection in retinal images is one such example and, therefore, requires some kind of adaptive local thresholding.

In this paper, we propose a general framework of adaptive local thresholding using a verification-based multithreshold probing scheme. Basically, it is assumed that, given a binary image B_T resulting from some threshold T, we are able to decide if any region in B_T can be accepted as an object by means of a classification procedure. In a more sophisticated manner, we even allow the classification procedure to accept part of a region. The operation is performed on a series of different thresholds and the final segmentation is obtained by combining the results from the individual thresholds. Overall, our approach adopts the paradigm of hypotheses generation and verification. Object hypotheses are generated by binarization using some hypothetic thresholds and accepted/rejected by the classification procedure.

The classification procedure is the core part of our framework that depends on the particular application. Here, we are able to incorporate any relevant information about objects, including shape, color/intensity, and contrast. In this sense, our approach can be regarded as knowledge-guided adaptive thresholding, in contrast to the vast majority of known thresholding algorithms based on statistical methods.

- *X. Jiang is with the Department of Electrical Engineering and Computer Science, Technical University of Berlin, D-10587 Berlin, Germany. E-mail: jiang@cs.tu-berlin.de.*
- *D. Mojon is with the Department of Neuro-Ophthalmology and Strabismus, Kantonsspital St. Gallen, CH-9007 St. Gallen, Switzerland. E-mail: daniel.mojon@kssg.ch.*

Manuscript received 13 Aug. 2001; revised 25 Mar. 2002; accepted 12 June 2002.
Recommended for acceptance by R. Beveridge.
For information on obtaining reprints of this article, please send e-mail to: tpami@computer.org, and reference IEEECS Log Number 114765.

In the rest of the paper, we first discuss the related literature. Then, our verification-based multithreshold probing framework is described in Section 3. Its application to vessel detection in retinal images is documented in Section 4. Finally, some discussions conclude the paper.

2 Related Works

Plenty of, particularly global, thresholding algorithms have been reported in the literature. The readers are referred to [11] for a most recent review. Only very few adaptive local approaches [1], [2], [8], [12] are known in the literature.

Our work shares with [9], [10] the use of multithreshold probing. O'Gorman [9] bases his approach on a histogram of the number of horizontal and vertical runs that result from thresholding the input image at a series of thresholds. Alternatively, Pikaz and Averbuch [10] investigate the histogram of the number of objects of some minimum size by applying binarization at different thresholds. It is important to mention that both approaches [9], [10] intend to determine a single global threshold, while our work leads to an adaptive local thresholding framework.

Probing the values of a parameter has also been used in other contexts. To adaptively close gaps in an edge map to form closed regions, various edge strengths are used to generate region hypotheses that are verified by means of statistical surface tests [6]. The same task is tackled in [4] by morphologically dilating edge maps. The probing parameter there is the number of dilation operations.

3 Verification-Based Multithreshold Probing

We assume that the images contain dark objects and bright background. Therefore, thresholding at a particular threshold T leads to a binary image B_T in which pixels with intensity lower than or equal to T are marked as object pixels and all other pixels as background. The description of our approach under this assumption, however, can be easily adapted to handle images of bright objects and dark background.

We introduce the verification-based multithreshold probing method by means of a simple example. The image shown in Fig. 1a consists of a uniform background of intensity 255, a circular object and a square object of intensity 20 and 200, respectively. Any threshold $T < 20$ leads to an empty binary image B_T, i.e., B_T contains only background pixels. On the other hand, the circular object is marked as object pixels for any threshold $20 \leq T < 200$, Fig. 1b. Similarly, any threshold $200 \leq T < 255$ marks both the circular and the square object as object pixels, Fig. 1c. Suppose we are looking for circular objects and we can design a verification procedure P_c which tells us if an image region is a true circular one. We perform a component labeling operation on each binary image B_T and carry out the test P_c on all connected regions. A new binary image B_T^* is obtained by retaining those regions which survive the test P_c. Then, B_T^* will contain circular regions only. In the case of the example in Fig. 1, $B_T^*,\ T < 20$ remains empty as B_T. Also, $B_T^* = B_T,\ 20 \leq T < 200$, holds. For $200 \leq T < 255$, B_T^* only contains the circular region while the square region is eliminated by the verification procedure P_c. Essentially, B_T^* retains those objects which we are interested in and are detectable at the particular threshold T. Finally, a logical OR operation of all B_T^* provides the overall thresholding result.

More formally, our verification-based multithreshold probing framework for adaptive local thresholding is specified in Fig. 2. Note that the output of the algorithm is not a dense threshold map, but a segmentation map of object and background pixels. Fundamental to our approach, thus the real challenge in actually applying it is the design of the application-dependent verification

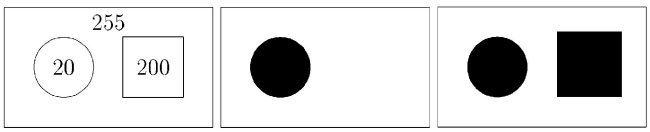

Fig. 1. Verification-based multithreshold probing: Regions survive the verification test as a whole or are eliminated. (a) Input image I. (b) Binary image $B_T,\ 20 \leq T < 200$. (c) Binary image $B_T,\ 200 \leq T < 255$.

procedure. Here, we can fully utilize the domain-specific knowledge by encoding any relevant information about objects including shape, color/intensity, and contrast. Properties such as scale and orientation invariance, if required by the particular task under consideration, must be taken into account as well. Considering the example in Fig. 1 again, if we are looking for square objects, we only need to replace the verification procedure P_c by some P_s which tests image regions for square shape. In order to detect both circular and square objects, a unification of P_c and P_s should be used. Generally, any verification procedure suitable for the particular task under consideration can be applied. Some examples are rule-based decision, decision tree, statistical classifiers, and neural network.

So far, we implicitly assumed that the verification test accepts or rejects an image region as a whole. This restriction has been made merely for description clarity and can be relaxed in general. Consider the situation in Fig. 3 where we are again interested in circular objects. Here, however, the single circular object is connected to another rectangular object due to overlapping. The verification test P_c as described before would fail in this case. The solution lies in a more sophisticated verification test P_c^* which is able to recognize that the image region resulting from thresholding at $20 \leq T < 255$, as shown in Fig. 3b is perfectly circular if the rectangular part is deleted. More generally, the verification test should detect some subregion(s) corresponding to the objects we are looking for from a thresholded image region. Certainly, it still has the possibility of accepting or rejecting an image region as a whole. Although usually more difficult to design, the second form of verification test may be very useful in practice. Later, in Section 4, we will describe its application to blood vessel detection in retinal images.

Besides the verification test, the set T_S of probe thresholds must be specified in order to adopt our framework in a particular application. In the simplest form, T_S takes values ranging from the minimum intensity $I_{\min}$ to the maximum intensity $I_{\max}$ of an image at some constant step. It may make sense to sample the range $[I_{\min}, I_{\max}]$ nonuniformly. For example, the sampling may be increasingly denser when moving from $I_{\min}$, respectively, $I_{\max}$ to the middle part of intensities. Essentially, any sampling scheme can be used if it is reasonable for the particular application.

The efficiency of our algorithm is mainly influenced by two factors: the verification test and the number of probe thresholds, i.e., $|T_S|$. Note that the operations for the probe thresholds are totally independent from each other and, therefore, the for-loop in Fig. 2 gives a perfect parallel structure. By simultaneously running these independent processes on parallel computers the computational time can be substantially reduced.

We want to point out that both the examples in Figs. 1 and 3 are merely strongly simplified cases used to introduce our approach. For these two situations with uniform background, a global thresholding may be applied to first yield a binary image which can be then checked by means of the verification test to find objects of interest. However, in the case of nonuniform background (e.g., increasing from dark on the left side to bright on the right side in Fig. 1), this simple method will not work. For this, and other more complex situations, in practice only approaches of some degree of adaptive behavior have a chance of success.

A popular strategy of adaptive thresholding [8] is to compute thresholds for subimages and to perform an interpolation for a dense map of individual thresholds for all pixels. Fig. 4 reveals a fundamental problem for this class of methods if there are abrupt changes in background. Two squares are to be detected on very different background; this situation has some similarity to normal and abnormal (pathological) areas of retinal images in our study. If the image is divided into two subimages, we obtain two thresholds. Here, we simply assume the threshold for the left (right) subimage be 60 (220). A linear interpolation of these values at center of the subimages would result in a threshold 140 at the border of the two subimages. The right (left) margin of the left (right) square is assigned a threshold 100 (180). Using these thresholds, traditional adaptive thresholding like [8] fails to correctly detect the squares in this case. On the other hand, using the verification procedure P_s our multithreshold approach is able to process this image properly.

4 Application to Vessel Detection in Retinal Images

Accurate detection of blood vessels in retinal images (see Fig. 5 for two examples) is important for a variety of tasks. Various approaches have been proposed for blood vessel detection; see [3] for a discussion.

4.1 Algorithm

We apply the verification-based multithreshold probing framework to detect vessels. From the methodology point of view, our

Input: intensity image I
set T_S of probe thresholds
Output: binary image B of object and background pixels

for each $T \in T_S$ **do** {
obtain binary image B_T by thresholding I at T;
apply verification procedure to B_T, obtaining binary image B_T^*
consisting of surviving whole/partial regions;
}
$B = \cup_{T \in T_S} B_T^*$;

Fig. 2. Adaptive local thresholding algorithm.

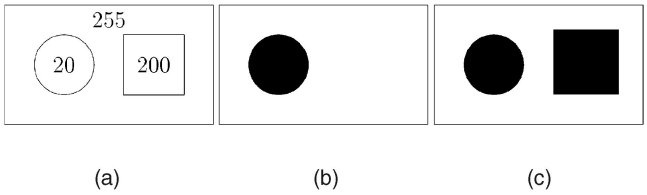

Fig. 3. Verification-based multithreshold probing: regions partially survive the verification test or are eliminated. (a) Input image I. (b) Binary image B_T, $20 \leq T < 255$. (c) Binary image B_T^*, $20 \leq T < 255$.

algorithm is therefore very different from previous approaches. The nature of retinal images (both nonuniform intensities of vessels and background) does not allow global thresholding techniques to be used. This is illustrated in Fig. 6, where two different thresholds make different parts of the vessel network visible.[1] The fundamental observation here is that a particular part of the vessel network can be well marked by some appropriate threshold which is, however, not known in advance. This motivates us to probe a series of thresholds and to detect vessels in the binary image resulting from the respective threshold. These partial results are then combined to yield an overall vessel network.

At this place, one comment is in order. A popular technique in dealing with nonuniform background is shade correction, which enables global operators to be carried out with some success. The main difficulty in applying this technique in our context is that retinal images may have a large portion of abnormal areas and this typically leads to abrupt changes in shading, as is the case in some of our test images. For this reason, we do not apply any shade correction technique to preprocess retinal images.

Thresholding with a particular threshold T leads to a binary image B_T, in which a pixel with intensity lower than or equal to T is marked as a vessel candidate and all other pixels as background. Vessels are considered to be *curvilinear structures* in B_T, i.e., lines or curves with some limited width. Here, it is crucial to design a verification (detection) procedure that detects such curvilinear structures in B_T and eliminates all other pixels. Our approach to vessel detection in B_T consists of three steps: 1) perform an Euclidean distance transform on B_T to obtain a distance map, 2) prune the vessel candidates by means of the distance map to only retain center line pixels of curvilinear bands, 3) reconstruct the curvilinear bands from their center line pixels. The reconstructed curvilinear bands give that part of the vessel network that is made visible by the particular threshold T. In the following, the three steps are described in detail.

We apply the fast algorithm for Euclidean distance transform from [5]. For each candidate vessel point, the resulting distance map contains the distance to its nearest background pixel and the position of that background pixel.

The pruning operation is the most crucial step in our approach. We use two measures, ϕ and d, introduced in [7] to quantify the likelihood of a vessel candidate being a center line pixel of a curvilinear band of limited width. The meaning of ϕ and d can be easily understood in Fig. 7, where p and n represent a vessel candidate and one of the eight neighbors from its neighborhood N_p, respectively, e_p and e_n are their corresponding nearest background pixel. The two measures are defined by:

1. Note that retinal images are usually captured in full color. Using an RGB color model, the blue band is often empty and the red band is often saturated. Therefore, we only work with the green band of retinal images.

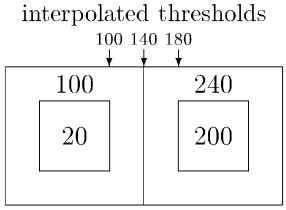

Fig. 4. Two squares on abruptly changing background.

$$\phi = \max_{n \in N_p} \text{angle}(\overline{pe_p}, \overline{pe_n}) = \max_{n \in N_p} \frac{180}{\pi} \cdot \arccos \frac{\overline{pe_p} \cdot \overline{pe_n}}{||\overline{pe_p}|| \cdot ||\overline{pe_n}||},$$
$$d = \max_{n \in N_p} ||\overline{e_p e_n}||.$$

The center line pixels of curvilinear bands typically have high values of ϕ. Therefore, our first pruning operation is based on a limit P_ϕ on ϕ. Since the blood vessels only have a limited width, which is approximated by d, we also put a limit P_d on d to only retain thin curvilinear bands.

Applying the two pruning operations above sometimes produces thin curvilinear bands that show only very weak contrast to the surrounding area and are not vessels. For this reason, we introduce a third photometric test by requiring a sufficient contrast. The contrast measure is defined by:

$$c = \max_{n \in N_p} \frac{\text{intensity}(q_n)}{\text{intensity}(p)},$$

where q_n ($\overline{pq_n} = P_{fac} \cdot \overline{pe_n}$, $P_{fac} > 1$) represents a pixel of the background in the direction $\overline{pe_n}$. The corresponding pruning operation is based on a limit $P_{contrast}$ applied to c.

After the three pruning operations, we obtain thin curvilinear bands, implicitly defined by their respective center line pixels. Sometimes, however, a few very short structures which are unlikely to be blood vessels are among the detected bands. Therefore, we impose a minimum size constraint. Connected components are labeled in the images containing the center line pixels and components smaller than P_{size} are removed.

In summary, we totally defined four pruning operations with respect to the properties angle (ϕ), width (d), contrast (c), and size. The remaining center line pixels surviving all tests, together with their respective distance values, can then be used to reconstruct the blood vessels that are made visible by the particular threshold T. This reconstructed binary image is actually B_T^*, the result of applying the overall verification test to B_T. A logical OR operation of B_T^* for all probe thresholds $T \in T_S$ provides the final result image with marked vessel points. In our experiments described below, we step through the intensity domain defined by the minimum and the maximum intensity of a retinal image at a fixed step T_{step}. Results with various values of T_{step} will be discussed. As an example, Fig. 8 shows the verification (detection) result B_{60}^* and B_{120}^* for the image in Fig. 6. Here, the parameter values $P_\phi = 135$, $P_d = 9$, $P_{fac} = 2.0$, $P_{contrast} = 1.07$, and $P_{size} = 37$ were used. For $T_{step} = 2$, the final result image is given in Fig. 9 (left).

So far, we have described the basic version of our algorithm for vessel detection. Now, we introduce two improvements to enhance the efficiency and the detection quality. Note that the three pruning operations with regard to angle, width, and contrast are carried out for each vessel candidate pixel in B_T. Since they have to consider all pixels of a local window, this is a relatively expensive step. Fortunately, a careful study of the geometry allows us to formulate a simple filter that can immediately eliminate a large portion of vessel candidates without the costly pruning operations. For each vessel candidate p, $||\overline{pe_p}|| \leq ||\overline{pe_n}||$ holds since e_p is the background pixel nearest to p. In addition, the center line pixels of

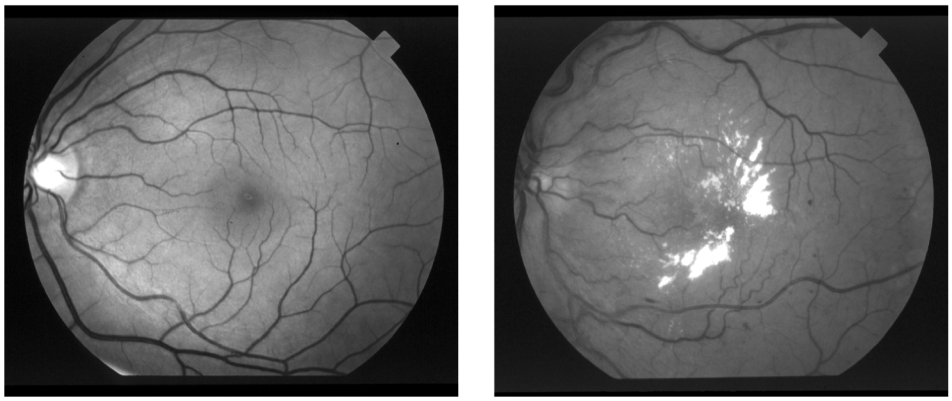

Fig. 5. A normal retinal image (left) and an abnormal retinal image (right).

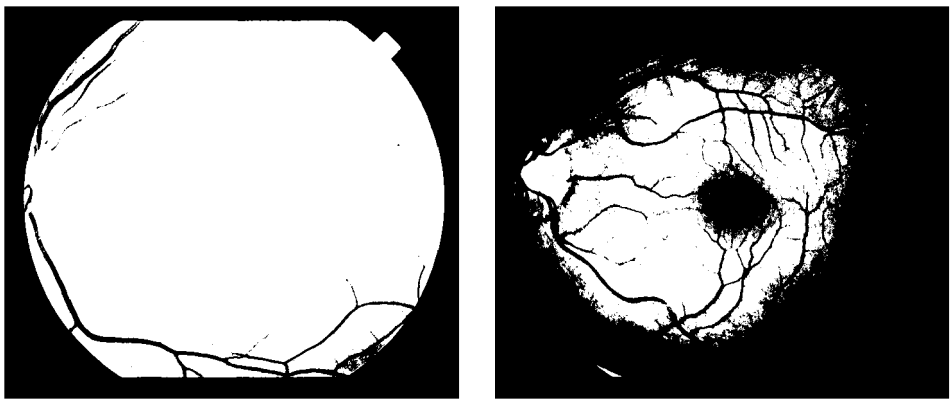

Fig. 6. For the normal retinal image in Fig. 5: thresholding results B_{60} and B_{120} from two thresholds 60 (middle) and 120 (right), respectively.

curvilinear bands have high values of ϕ; we require $\phi > \frac{\pi}{2}$ in our experiments. Considering these two facts, we obtain:

$$\begin{aligned} d &= \sqrt{||\overline{pe_p}||^2 - 2||\overline{pe_p}|| \cdot ||\overline{pe_n}|| \cos\phi + ||\overline{pe_n}||^2} \\ &\geq \sqrt{2||\overline{pe_p}||^2 - 2||\overline{pe_p}||^2 \cos\phi}. \end{aligned}$$

Because of the limit P_ϕ on ϕ, this is further reduced to:

$$d \;\geq\; \sqrt{2} \cdot ||\overline{pe_p}|| \cdot \sqrt{1 - \cos P_\phi}.$$

If the term on the right side is larger than the limit P_d, then p has no chance of surviving the width test on d at all and, therefore, can be safely ignored. This results in the filter:

$$\text{if } ||\overline{pe_p}|| > \frac{P_d}{\sqrt{2} \cdot \sqrt{1 - \cos P_\phi}} \text{ then eliminate } p.$$

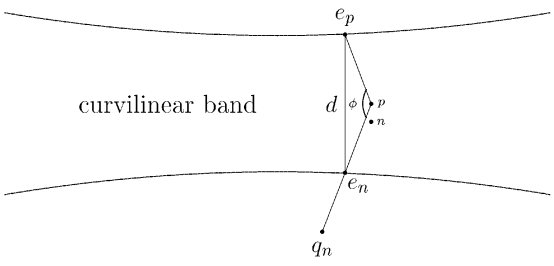

Fig. 7. Quantities for testing curvilinear bands.

It immediately eliminates a large portion of vessel candidates without investigating their neighborhood and only those surviving candidates are further checked by the more costly pruning operations. For relatively high probe thresholds which generate many vessel candidates, this filter turns out to be particularly effective.

A look at the vessel detection result shown in Fig. 9 (left) reveals that the vessel boundaries are not very clean. A postprocessing is added to solve this problem. Generally, pixels on vessel boundaries may be characterized as local maximum of intensity gradients. Based on this observation, we conduct the following nonmaxima suppression procedure. The Sobel operator is applied to compute both the magnitude and orientation of the gradient of all vessel pixels using the original input image. For each vessel pixel p adjacent to the background, we search for a vessel pixel p' in the neighborhood of p that has the same gradient orientation as p. If such a p' exists and the gradient magnitude of p is smaller than that of p', then p is deleted. This nonmaxima suppression procedure is repeated until no change more is possible. On the binary image resulting from the nonmaxima suppression, an opening and a subsequent closing operation are performed to obtain the final result image. In our experience, this postprocessing step largely improves the vessel boundaries, see Fig. 9 (right) for an example.

Our algorithm has five parameters: P_ϕ, P_d, P_{fac}, $P_{contrast}$, P_{size}. Among them, P_ϕ and P_d are responsible for finding the major part of the vessel network. The other three parameters have, to some degree, the character of postprocessing and contribute more to the refinement of detected vessels. Because of the different roles, P_ϕ and P_d tend to be more critical and should be chosen carefully.

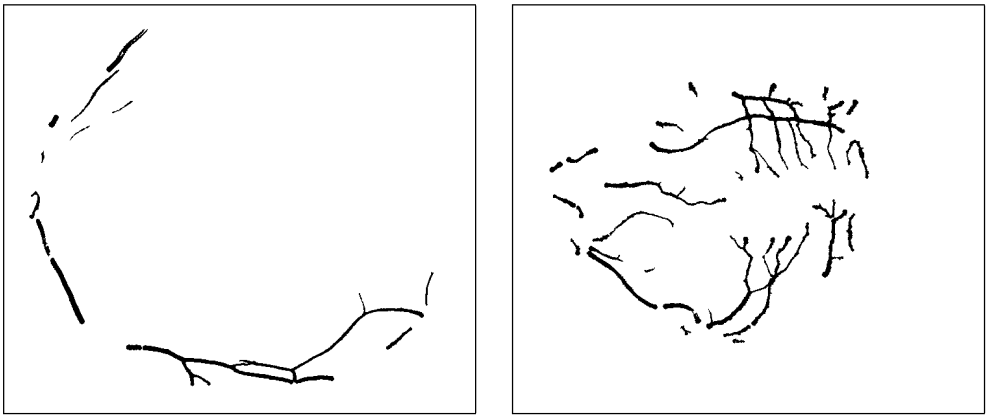

Fig. 8. For the normal retinal image in Fig. 5: verification (detection) result B^*_{60} (left) and B^*_{120} (right); compare to Fig. 6.

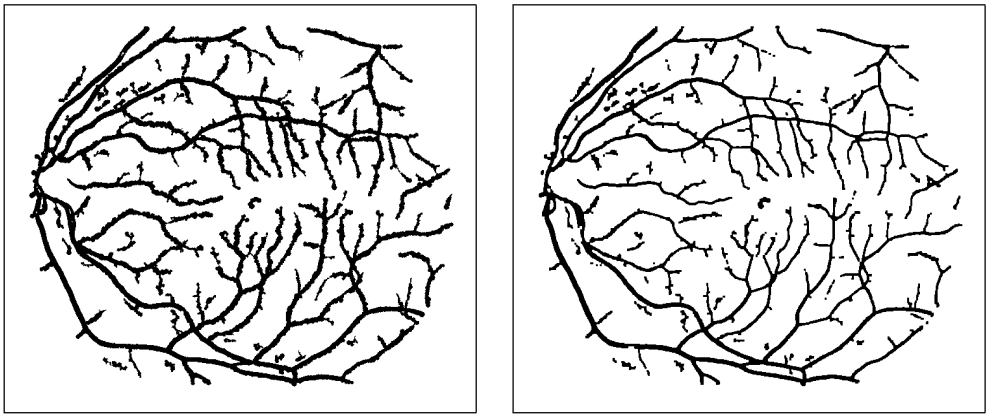

Fig. 9. For the normal retinal image in Fig. 5: detected vessels without postprocessing (left) and with postprocessing (right).

4.2 Experimental Evaluation

Our vessel detection algorithm has been implemented in C and tested under Linux on a Pentium III 600MHz PC. For two reasons we have chosen the set of 20 retinal images used in [3] for performance evaluation. First, the retinal images have all hand-labeled vessel segmentation and support quantitative evaluation in an objective manner. Second, the image set contains both normal and abnormal (pathological) cases. In contrast, most of the methods known from the literature have only been demonstrated upon normal vessel appearances, which are easier to discern. The 20 images were digitized from retinal fundus slides and are of 605×700 pixels, 24 bits per pixel (standard RGB). We only use the green band of the images.

Given a machine-segmented result image (MS) and its corresponding hand-labeled ground truth image (GT), the performance is measured as follows: Any pixel which is marked as vessel in both MS and GT is counted as a true positive. Any pixel which is marked as vessel in MS but not in GT is counted as a false positive. The true positive rate is established by dividing the number of true positives by the total number of vessel pixels in GT. The false positive rate is computed by dividing the number of false positives by the total number of nonvessel pixels in GT.

Our algorithm has five parameters: P_ϕ, P_d, P_{fac}, $P_{contrast}$, P_{size}. We report results using eight sets of parameter values: $P_\phi = 150 - 5k$, $P_d = 6 + k$, $P_{fac} = 2.0$, $P_{contrast} = 1.07$, $p_{size} = 46 - 3k$, $k = 0, 1, \ldots, 7$. The linear setting of parameter values was selected by some experiments and human judgment. Several functions similar to this setting were explored, by varying the initial values and increments. It was observed that these settings produced very similar results. Note that the example vessel detection result shown in Fig. 9 was achieved using parameter values at $k = 3$. Fig. 10 shows the average performance curve over the 20 images for the eight parameter sets. Here, $T_{step} = 2$ is used; the performance at various T_{step} values will be discussed later in this section.

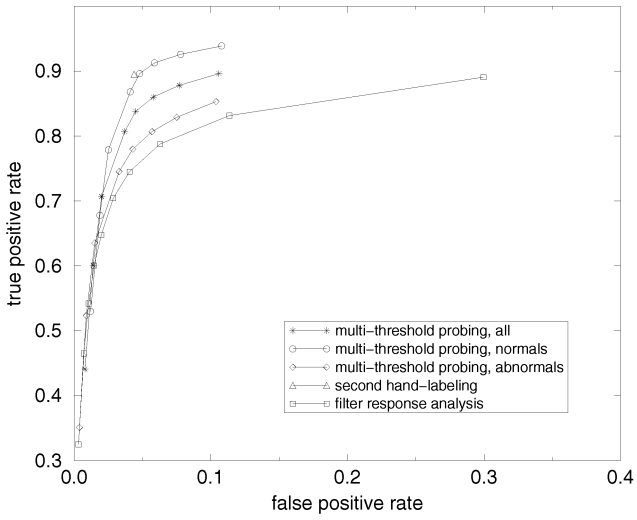

Fig. 10. Average performance over 20 images: our approach vs. filter response analysis method.

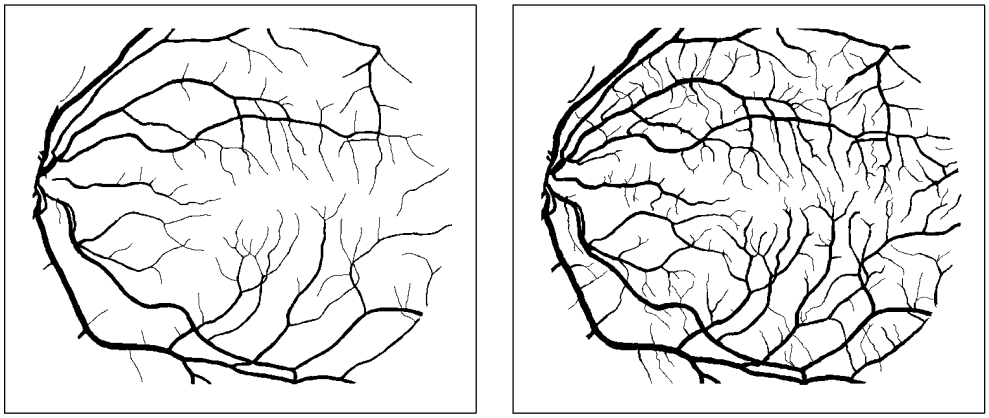

Fig. 11. Hand-labeled vessels segmentation for the normal image in Fig. 5 from two people.

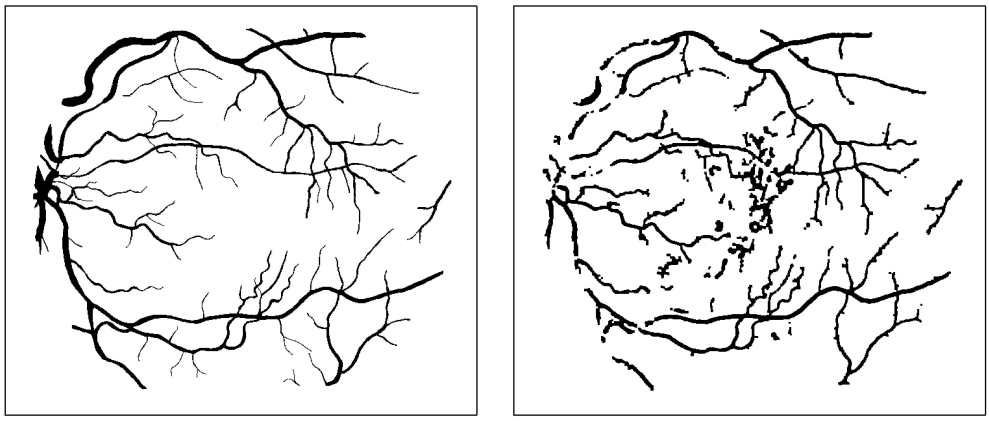

Fig. 12. For the abnormal retinal image in Fig. 5: first hand-labeling (left) and detected vessels after postprocessing (right).

For the 20 images, there are two hand-labelings made by two different people, see Fig. 11 for an example. The first hand-labeling, which is used as ground truth in our evaluation, took a more conservative view of the vessel boundaries and in the identification of small vessels than the second hand-labeling. By considering the second hand-labeling as "machine-segmented result images" and comparing them to the ground truth, we obtain a detection performance measure which is then regarded as a target performance level. This level is indicated by the isolated triangle mark in Fig. 10. Our algorithm produces the same number of false positives at a 83.4 percent true positive rate as the second set of hand-labeled images at a 89.5 percent true positive rate. This suggests room for an improvement of 6.1 percent in the true positive rate over our method.

As a reference, the average performance curve for the method based on filter response analysis [3] is drawn in Fig. 10. We observe similar performance up to approximately 65 percent true positive rate. For higher true positive rates, our approach clearly shows superior performance with respect to the false positive rate. As an example, the second hand-labeling gives a performance of 89.5 percent true positive rate at 4.4 percent false positive rate. To achieve the same true positive rate, our approach has a false positive rate which is slightly higher than doubling 4.4 percent, but

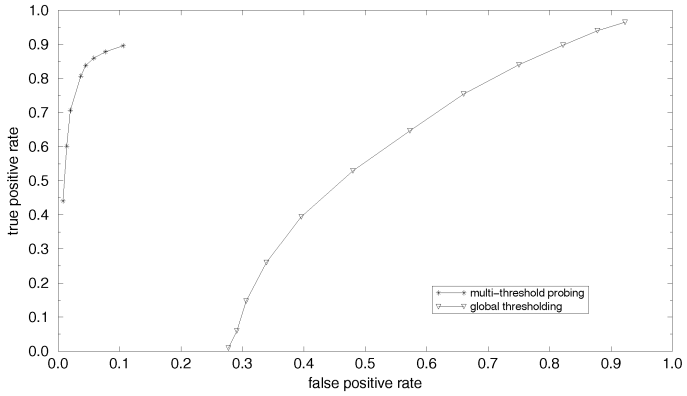

Fig. 13. Average performance over 20 images: our approach versus global thresholding.

much lower than that would be required by the filter response analysis method [3].

Among the 20 images, 10 are of patients with no pathology (normals) and the other 10 contain pathology that obscures or confuses the blood vessel appearance in varying positions of the image (abnormals); see Fig. 5 for a sample normal and abnormal retinal image and Figs. 9 and 12 for their vessel detection result. The availability of both normal and abnormal images allows us to investigate the algorithm performance on the two image classes separately, see Fig. 10. Since there is virtually no difference in the performance of the filter response analysis method [3] on normals and abnormals, only the overall average performance curve is drawn there as a reference. Our method demonstrates a superior performance on normals compared to abnormals. But, the performance on abnormals is still slightly better than that in [3].

Our multithreshold probing strategy is motivated by the fact that a single threshold only reveals part of the vessel network and, therefore, the traditional global thresholding cannot work well. This is quantitatively demonstrated by the average performance curve for the global thresholding in Fig. 13, established for the thresholds $40, 50, 60, \ldots, 150$. Consequently, no global thresholding technique is appropriate for this task.

The computational efficiency of our algorithm depends on the parameter T_{step}, the sampling density of probe thresholds. The performance study above is based on $T_{step} = 2$. A comparison of the average performance over 20 images for various T_{step} values indicates that there is virtually no difference in the performance. The average computation time including postprocessing is 36/19/13/10/8 seconds per image for $T_{step} = 1/2/3/4/5$. As expected, it approximately decreases in a linear manner with increasing T_{step} values. We conclude that, for the reason of efficiency, we may use a relatively sparse sampling of probe thresholds without noteworthy loss of vessel detection quality. Another remark is that, among all operations of the algorithm, the pruning operation is the most expensive one. It takes about 70 percent of the total computation time. We have suggested a filter to speed up this step. More efforts here have the largest potential to further reduce the computation time.

5 Conclusion

In this paper, we have proposed a general framework of adaptive local thresholding based on a verification-based multithreshold probing scheme. The application-dependent verification procedure can be designed to fully utilize all relevant information about the objects of interest. In this sense, our approach is regarded as knowledge-guided adaptive thresholding. It is our belief that only the full use of domain-specific knowledge will achieve success to the largest extent. Our work represents a step toward this direction.

Due to its simplicity and general nature, the verification-based multithreshold probing framework is expected to be applicable to a variety of other tasks. Potential applications are, for instance, the recognition and counting of pigmented skin lesions, microaneurysms in digital angiograms of the eye fundus, and microcalcification in mammograms.

Acknowledgments

The work was supported by the Stiftung OPOS Zugunsten von Wahrnehmungsbehinderten, St. Gallen, Switzerland. A preliminary version of this paper was presented at the German Conference on Pattern Recognition, Munich, 2001. The authors would like to thank A. Hoover at Clemson University for making the retinal image material and the ground truth data publically available and his comments on this work.

References

[1] J. Bernsen, "Dynamic Thresholding of Grey-Level Images," *Proc. Int'l Conf. Pattern Recognition*, pp. 1251-1255, 1986.
[2] C.K. Chow and T. Kaneko, "Automatic Boundary Detection of the Left Ventricle from Cineangiograms," *Computing Biomedical Res.*, vol. 5, pp. 388-410, 1972.
[3] A. Hoover, V. Kouznetsova, and M. Goldbaum, "Locating Blood Vessels in Retinal Images by Piece-Wise Threshold Probing of a Matched Filter Response," *IEEE Trans. Medical Imaging*, vol. 19, no. 3, pp. 203-210, 2000.
[4] X. Jiang, "An Adaptive Contour Closure Algorithm and Its Experimental Evaluation," *IEEE Trans. Pattern Analysis and Machine Intelligence*, vol. 22, no. 11, pp. 1252-1265, Nov. 2000.
[5] F. Leymarie and M. D. Levine, "Fast Raster Scan Distance Propagation on the Discrete Rectangular Lattice," *CVGIP: Image Understanding*, vol. 55, no. 1, pp. 84-94, 1992.
[6] S.-P. Liou, A.H. Chiu, and R.C. Jain, "A Parallel Technique for Signal-Level Perceptual Organization," *IEEE Trans. Pattern Analysis and Machine Intelligence*, vol. 13, no. 4, pp. 317-325, Apr. 1991.
[7] G. Malandain and S.F. Vidal, "Euclidean Skeletons," *Image and Vision Computing*, vol. 16, pp. 317-327, 1998.
[8] Y. Nakagawa and A. Rosenfeld, "Some Experiments on Variable Thresholding," *Pattern Recognition*, vol. 11, pp. 191-204, 1979.
[9] L. O'Gorman, "Binarization and Multithresholding of Document Images Using Connectivity," *CVGIP: Graphical Models and Image Processing*, vol. 56, no. 6, pp. 494-506, 1994.
[10] A. Pikaz and A. Averbuch, "Digital Image Thresholding Based on Topological Stable-State," *Pattern Recognition*, vol. 29, no. 5, pp. 829-843, 1996.
[11] B. Sankur and M. Sezgin, "Image Thresholding Techniques: A Survey Over Categories," *Pattern Recognition*, under review.
[12] S.D. Yanowitz and A.M. Bruckstein, "A New Method for Image Segmentation," *Computer Vision, Graphics, and Image Processing*, vol. 46, pp. 82-95, 1989.